1664–1675 *Nucleic Acids Research, 2010, Vol. 38, No. 5* *Published online 11 December 2009*
doi:10.1093/nar/gkp1104

PCNA and XPF cooperate to distort DNA substrates

Richard D. Hutton[1], Timothy D. Craggs[2], Malcolm F. White[1,*] and J. Carlos Penedo[1,2,*]

[1]Centre for Biomolecular Sciences and [2]School of Physics and Astronomy, University of St Andrews, North Haugh, St Andrews, KY16 9SS, UK

Received October 2, 2009; Revised and accepted November 9, 2009

ABSTRACT

XPF is a structure-specific endonuclease that preferentially cleaves 3′ DNA flaps during a variety of repair processes. The crystal structure of a crenarchaeal XPF protein bound to a DNA duplex yielded insights into how XPF might recognise branched DNA structures, and recent kinetic data have demonstrated that the sliding clamp PCNA acts as an essential cofactor, possibly by allowing XPF to distort the DNA structure into a proper conformation for efficient cleavage to occur. Here, we investigate the solution structure of the 3′-flap substrate bound to XPF in the presence and absence of PCNA using intramolecular Förster resonance energy transfer (FRET). We demonstrate that recognition of the flap substrate by XPF involves major conformational changes of the DNA, including a 90° kink of the DNA duplex and organization of the single-stranded flap. In the presence of PCNA, there is a further substantial reorganization of the flap substrate bound to XPF, providing a structural basis for the observation that PCNA has an essential catalytic role in this system. The wider implications of these observations for the plethora of PCNA-dependent enzymes are discussed.

INTRODUCTION

Structure-specific endonucleases recognise and cleave a variety of branched structures that arise during DNA replication, recombination and repair (1,2). In eukarya, the nuclease xeroderma pigmentosum complementation group F (XPF), which forms a complex with the excision repair cross complementary group 1 (ERCC1) protein, is a component of the eukaryotic nucleotide excision repair (NER) machinery and cleaves a 3′ single-stranded flap structure on the 5′ side of DNA lesions (3). In humans, mutation of XPF can cause xeroderma pigmentosum (XP), which is characterized by extreme sensitivity to UV light and a high frequency of skin cancer (4). In crenarchaea, XPF forms homodimers composed of nuclease and helix–hairpin–helix (HhH_2) domains connected by a short linker (5–7). The crystal structure of the *Aeropyrum pernix* XPF (ApeXPF), both bound to a dsDNA and in an unliganded form, revealed important features of substrate recognition and cleavage of branched DNA structures by these proteins (8). The structure revealed that the nuclease and HhH_2 domains independently form tightly associated dimers with equivalent domains. The dimeric HhH_2 domains were predicted to bind the DNA substrate, inducing a 90° bending angle between the downstream and upstream duplexes (8). This is similar to what was observed for the RuvA tetramer bound to a planar Holliday junction (9). This DNA substrate rearrangement is also accompanied by a large inter-domain movement, with a 30 Å shift and 95° rotation occurring in the protein. In a parallel study, Nishino *et al.* (6) proposed a broadly similar model for the recognition of the fork substrate by the euryarchaeal version of XPF (Hef).

A major conformational change in the DNA structure has been also reported for the interaction between the 5′ flap endonuclease Fen-1 and DNA substrates using fluorescence resonance energy transfer (FRET). The decrease in the distance between the ends of the DNA supported a kink angle of ~90°–100° with the kink centred at the phosphate opposite the flap junction (10). *In vitro*, Fen-1 activity is increased by up to 50-fold in the presence of the sliding clamp PCNA (11,12), a ring-shaped protein that encircles DNA and acts as a platform for the recruitment of a variety of non-sequence-specific enzymes including polymerases, nucleases, helicases and glycosylases (13,14). We have shown previously that *Sulfolobus solfataricus* XPF has significant endonuclease activity only in the presence of the heterotrimeric crenarchaeal PCNA (5,15,16). Crystal structures of heterotrimeric *S. solfataricus* PCNA on its own (18) and in complexes with Fen-1 (19,20) and DNA ligase (20) have revealed a close resemblance to homotrimeric eukaryotic and euryarchaeal orthologs.

*To whom correspondence should be addressed. Tel: +44 1334 463106; Fax: +44 1334 463104; Email: jcp10@st-andrews.ac.uk
Correspondence may also be addressed to Malcolm F. White. Tel: +44 1334 463432; Fax: +44 1334 462595; Email: mfw2@st-andrews.ac.uk

Using a continuous FRET assay we demonstrated that *S. solfataricus* PCNA activated the XPF and Fen-1 nucleases by two fundamentally different mechanisms and proposed a novel role for PCNA as an essential XPF cofactor (21). For Fen-1, PCNA activation mainly arises from an increased affinity for DNA, which represents the accepted role of PCNA. In contrast, for XPF, PCNA increases the catalytic rate constant by almost four orders of magnitude without affecting the K_M, indicating that PCNA seems to reduce the activation barrier of the catalytic reaction.

In the absence of a crystal structure of the XPF/DNA/PCNA complex, our current knowledge of XPF interactions with DNA and PCNA is limited. Here, we analyse the conformational changes occurring on the flap substrate upon binding to XPF and the XPF/PCNA complex using FRET. Analysis of these conformational changes has revealed, for the first time, substantial differences for the structure of the flap DNA substrate bound to the XPF nuclease in the presence and absence of PCNA, and suggest a role for the PCNA sliding clamp as an architectural organiser of the XPF/DNA complex.

MATERIALS AND METHODS

Protein expression and purification

S. solfataricus wild-type and the C terminal truncated Δ6 XPF and PCNA heterotrimer were expressed and purified as described previously (16,17). The HhH_2 domain of XPF was amplified from *S. solfataricus* strain P2 genomic DNA using the following primers:

5′ primer: 5′-CGTCGGATCCCCCATGGCTAAATTG GAAAGTGTTTCTG.
3′ primer: 5′-CCGGGGATCCGTCGACCTAAAGGAA ATCAAATAAAG

The PCR product was cloned into using *Sal*1/*NcoI* recognition sites of the vector pET28c (Novagen) for his-tagged recombinant protein expression and sequenced. Expression was carried out in BL21 Rosetta (DE3) cells induced by adding 0.2 mM IPTG when cultures reached A_{600} 0.7, grown for further 3 h and the cells pelleted. The bacterial pellet was resuspended in ~35 ml buffer (20 mM sodium phosphate, pH 7.4, 500 mM NaCl and 1 mM benzamidine) and sonicated 4 × 2 min with cooling. The lysate was centrifuged at 48 000 *g* for 20 min, 4°C and the supernatant heated to 70°C to precipitate *E. coli* proteins before centrifugation for a further 20 min. The supernatant was applied to a Nickel chelating column (HiTrap™ 5 ml Chelating HP, GE Healthcare) and eluted with a linear gradient of imidazole (0–0.5 M). The fractions containing HhH_2 were identified by SDS–PAGE, pooled and concentrated to ~7 ml and loaded onto a HiLoad® 26/60 Superdex® 200 gel filtration column (GE Healthcare) equilibrated with buffer (20 mM MES pH 6.0, 1 mM EDTA, 0.5 mM DTT, 150 mM NaCl). Fractions corresponding to the peak were concentrated as before and the protein concentration calculated from the extinction coefficient at 280 nm. SDS–PAGE confirmed the protein was essentially pure. Protein stocks were stored at −80°C in 15% glycerol until required.

Oligonucleotide labelling and purification

Oligonucleotides were purchased from Integrated DNA Technologies labelled with the donor dye fluorescein or/and an internal amino modifier C6-dT. A succinimidyl ester derivative of the fluorophore Cy3 (GE Healthcare) was used according to the manufacturer's protocol for the specific labelling of the DNA oligonucleotides. Following the labelling reaction, the oligonucleotide was ethanol precipitated followed by a 70% ethanol wash before being allowed to dry. The pellet was re-suspended in 200 µl of 50% formamide and incubated at 55°C for 5 min before loading on to a pre-run 20% denaturing acrylamide gel at 22 W (limited to 55°C using a temperature probe) for 3 h. Bands were visualized by UV-shadowing, cut and then extracted from the gel using an overnight crush and soak protocol at 4°C (CSH Protocols, 2006; doi:10.1101/pdb.prot2936), followed by ethanol precipitation. The absorption spectrum from 600–220 nm was taken to determine DNA concentration and labelling efficiency of the fluorescent dyes. To provide a DNA scaffold that could act efficiently as substrate for the XPF/PCNA complex, given that the footprint of XPF into DNA extends ~7–8-nt from the nicked site (8) and that PCNA is expected to require ~10 bp DNA duplex for binding, the length of each DNA stem was set at 19 and 18 bp for the up- and downstream regions, respectively. The 3′-flap substrate was assembled using 0.1 OD of each strand (Table 1) and hybridized as described previously (21).

Fluorescence binding assay

Binding experiments were performed in 30 mM HEPES, pH 7.6, 40 mM KCl, 5% glycerol, 0.1 mg/ml bovine serum albumin with 50 nM DNA substrate. For experiments performed in the presence of PCNA, addition of the clamp loader RFC was not required as PCNA can readily diffuse on to the short synthetic DNA substrates used in this study. Experiments were performed using a Cary Eclipse spectrofluorimeter (Varian Inc., Palo Alto, USA), equipped with a Peltier temperature controller set to 20°C. FRET measurements were performed under magic angle conditions to avoid anisotropy effects and analysed by exciting the donor dye fluorescein at 490 nm recording the emission spectrum from 500 to 650 nm. The acceptor dye (Cy3) emission spectrum was also recorded using an excitation wavelength of 545 nm and emission monitored from 557 to 650 nm. Anisotropy measurements were recorded using the automated polariser accessory using a 5 s averaging time and four replicates for each measurement (λ_{ex} = 490 nm, λ_{em} = 535 nm). Differences in the fluorimeter response to vertical and horizontal polarized light (G-factor) were corrected automatically by the spectrofluorimeter. Dissociation constants were calculated by non-linear least-squares fitting of the raw data to the standard equation describing the equilibrium $D + E \leftrightarrow DE$ (D is the oligonucleotide, E is

Table 1. Oligonucleotides used for DNA substrates

	Oligonucleotide	Sequence (5′–3′)
	XPF-A[a]	AGCCCGACAGCAGTCAGAGCTTGCTAGGACGGACGGT
Flap-12	XPF12-B	ACCGTCCG[iFluorT]CCTAGCAAGCATTTTTTT[3AmM][b]
	XPF12-C	TCTGACTGCTGTCGGGCT
Flap-13	XPF13-B	ACCGTCCG[iAmMC6T]CCTAGCAAGCATTTTTTT[c]
	XPF-C[d]	TCTGACTGC[iFluorT]GTCGGGCT[d]
Flap-23	XPF23-B	ACCGTCCGTCCTAGCAAGCATTTTTTT[3Cy3][e]

[a]XPF-A is common to all the flaps studied.
[b][iFluorT] (internal fluorescein FRET donor), [3AmM] (3′ amino modifier).
[c][iAmMC6T] (internal amino modifier with six carbon linker).
[d]XPF-C was used in Flap-13 and Flap-23.
[e][3Cy3] (3′ modification with Cy3 FRET acceptor).

the protein and DE is the oligonucleotide–protein complex).

$$A = A_{\min}[(D + E + K_D) - \{(D + E + K_D)^2 - (4DE)\}^{1/2}(A_{\max} - A_{\min})/(2D), \quad \mathbf{1}$$

where A represents the measured signal at a particular protein concentration (E) and fluorescent oligonucleotide (D), $A_{\min}$ indicates the minimum signal value, $A_{\max}$ represents the maximum signal value and K_D is the dissociation constant. Assuming that for a given protein the changes in FRET efficiency observed for the three flap constructs are induced by the same type of protein–DNA interaction, global analysis was carried out using also Equation (1) but with the K_D being optimized as a global parameter with a single value for all the flap constructs.

Determination of FRET efficiencies and distances

The efficiency of energy transfer from the donor (fluorescein) to the acceptor (Cy3) was calculated following the $(\text{ratio})_A$ method (22). It is commonly found that when proteins bind to fluorescent constructs, potential changes in the fluorescence intensity of the donor and/or the acceptor may occur due to changes in the local environment of the fluorophores (23,24). Changes in acceptor and donor quantum yield do not interfere with the calculation of the FRET efficiency following the $(\text{ratio})_A$ method. However, because the quantum yield of the donor enters directly into calculations of the Förster energy transfer distance (R_o), this must be taken into account when comparing FRET values in absence and presence of different protein concentrations and particularly, when transforming the experimental FRET efficiency to distance values (22,24). Corrected FRET efficiencies and distance values have been obtained following procedures reported in the literature (25). Briefly, for each data point in a titration experiment, the percentage of protein-induced donor quenching was assessed under the same experimental conditions using a donor-only construct. Thus, the corrected distance can be calculated from the expression:

$$R = R_o\left(\frac{\Phi_D^{\text{protein}}}{\Phi_D}\right)^{1/6}\left(\frac{1}{E_{\text{exp}}} - 1\right)^{1/6}, \quad \mathbf{2}$$

where R_o represents the Förster distance in the absence of protein (55.6 Å), $\phi_D^{\text{protein}}/\phi_D$ indicates the ratio between the donor emission at each protein concentration and in the donor-only construct, and E_{exp} is the experimental FRET efficiency obtained following the $(\text{ratio})_A$ method.

Angle calculations using a single- and a double-kink DNA model

The dye-to-dye distance obtained from FRET efficiency measurements was correlated with conformational changes within the DNA substrate upon XPF and XPF/PCNA binding by calculating the DNA kink angle α using a single-kink model (26). The kink centre was assumed to be at the phosphate opposite the ss/dsDNA junction and flanked, for Flap-13, by 11 bp (L_1) and 10 bp (L_2) duplex DNA regions, which represent the position of the dyes in the upstream and downstream duplexes, respectively. For Flap-12, L_1 and L_2 take the values 11 bp duplex DNA and 8 nt of single-strand DNA, and for Flap-23 the values of 10 bp (L_1) and 8 nt ssDNA (L_2). Duplex DNA length was calculated assuming canonical B-DNA and for ssDNA length we used the limiting values reported in the literature of 4 and 5.6 Å for the inter-base distance and also the value of 5.3 Å obtained from the average of six crystal structures of ssDNA/protein complexes (see text). The angle α was calculated for each FRET vector from $\cos(\alpha) = [(R_{\text{FRET}}^2 - L_1^2 - L_2^2)/2L_1L_2]$.

To explore the compatibility of the FRET distances obtained with a model including XPF-induced melting of the DNA template, we also applied a double-kink model (23). In this case the DNA substrate is treated as a rigid rod with three segments, L_{up} (upstream duplex length), L_{down} (downstream duplex length) and L_m (single-strand DNA region linking the upstream and downstream), and two 'hinges' that separate the three segments (Figure 4d). The total kink angle between the upstream and downstream region is $\alpha = 2\theta$, where θ represents the exterior angle at each ss/dsDNA interface. L_{up} and L_{down} are given by the expressions $L_{\text{up}} = (11\text{ bp} - L_m) \times 3.4\text{ Å}$, and $L_{\text{down}} = 10\text{ bp} \times 3.4\text{ Å}$. Assuming no twisting of the construct, all three segments lie at the xy plane with the position of the

upstream dye at the origin of a coordinate system and the position of the downstream dye is defined by the expressions:

$$x = L_{up}\cos\theta + L_m + L_{down}\cos\theta, \quad 3$$

$$y = L_{up}\sin\theta - L_{down}\sin\theta. \quad 4$$

The dye-to-dye distance in the protein–DNA complex is given by $R_b^2 = x^2 + y^2$. By applying these equations, we estimate the L_m value taking α as 90°, assuming symmetric kink at each ss/dsDNA interface (θ as 45°) and assigning the distance, R_b, as the experimentally obtained distance by FRET measurements.

RESULTS

XPF directs PCNA loading onto 3′flap DNA substrates

Although PCNA is known to associate with DNA flap substrates, it has not yet been possible to determine a structure of an isolated PCNA/DNA complex by crystallographic methods and its relative upstream or downstream DNA binding orientation in the presence and absence of XPF remains unclear. We have shown previously that a 3′flap DNA structure labelled internally with fluorescein is an adequate substrate for XPF with catalytic rates similar to that obtained from an unlabelled substrate (21). Here, we have used PCNA-induced quenching of internally labelled fluorescein emission to determine the affinity constant of PCNA for a DNA flap structure and its relative orientation in the presence and absence of XPF. Fluorescein dyes were located either 11 nucleotides upstream or 10 nucleotides downstream of the 3′ flap junction on the substrate (Figure 1a) and PCNA titrations were carried out in a background of 10 mM Ca^{2+} to prevent cleavage. As for other divalent metal-ion dependent endonucleases, Ca^{2+} ions have been demonstrated to inhibit the catalytic step while efficiently stabilizing protein–DNA interactions (3,27). In the absence of XPF, both the upstream and downstream fluorescein dyes exhibited a similar degree of quenching (~30%) on PCNA binding and similar dissociation constants of 8.5 ± 1.6 and 6.9 ± 1.8 μM (Figure 1b), respectively. For comparison, K_D values of 1 μM for the binding of homotrimeric yeast PCNA to a 24 bp dsDNA and ~100 μM to a 50 bp dsDNA carrying a 5-nt overhang have been obtained using a quartz crystal microbalance approach (28). Titration of PCNA with DNA pre-equilibrated with 1 μM wild-type XPF showed a remarkably different behaviour. No quenching was observed for the downstream fluorescein, suggesting that PCNA cannot bind there in the presence of XPF (Figure 1b). For the upstream duplex, ~75% quenching of the fluorescence signal was observed and a K_D of 36 ± 7 nM was measured, representing an ~200-fold decrease in the dissociation constant when compared to PCNA alone. These data confirm that in the XPF–PCNA–DNA ternary complex PCNA binds the DNA duplex that is upstream (5′ to the flap), as predicted by McDonald and colleagues (8).

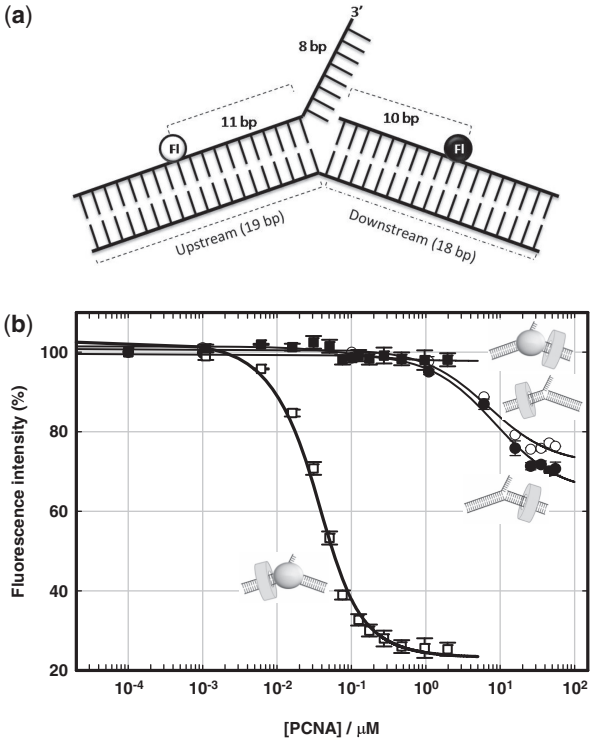

Figure 1. PCNA loading onto flap substrates is directed by XPF. (**a**) Schematic of the DNA constructs used to monitor PCNA assembly onto the flap susbtrate. Two DNA constructs were post-synthetically labelled with fluorescein positioned either on the upstream duplex, 11-nt from the 3′ flap ds/ss junction, or on the downstream duplex, 10-nt from the ds/ss junction. (**b**) Percentage quenching at 20°C and 10 mM $CaCl_2$ of an upstream (white) and a downstream (black) fluorescein-labelled flap substrate as a function of PCNA concentration in the presence (squares) and absence (circles) of XPF. The data were fitted with a simple one site binding model, yielding a binding stoichiometry of 1:1 and a K_D of 8.5 μM (upstream) and 6.9 μM (downstream) in the absence of XPF. In the presence of 1 μM XPF no quenching was observed for the downstream location and a K_D of 36 nM was obtained for the upstream-labelled substrate.

XPF affinity for 3′flap substrates using a FRET-based assay

We have previously reported a dissociation constant of 3.8 ± 0.6 μM and a 1:1 stoichiometry for the XPF/PCNA complex using isothermal titration calorimetry (21); however, binding affinities of XPF and XPF/PCNA for DNA substrates have not been reported to date. Here, we used an intramolecular FRET assay to quantify the affinity of wild type XPF (XPF-wt) and truncated variants lacking the C-terminal PCNA-interacting peptide (XPF-ΔPIP), or the nuclease domain (XPF-Δnuc), for the 3′flap DNA substrate, in the presence and absence of PCNA. Three FRET constructs were engineered carrying the donor (fluorescein) and the acceptor dye (Cy3) at different positions (Figure 2, top panel). Two of these constructs reported structural distortions involving the 8-nt single-strand flap and the upstream (Flap-12) or downstream (Flap-23) duplexes, whilst Flap-13 monitors changes in the kink angle between both duplex arms. FRET binding curves were obtained at room temperature by titrating each FRET

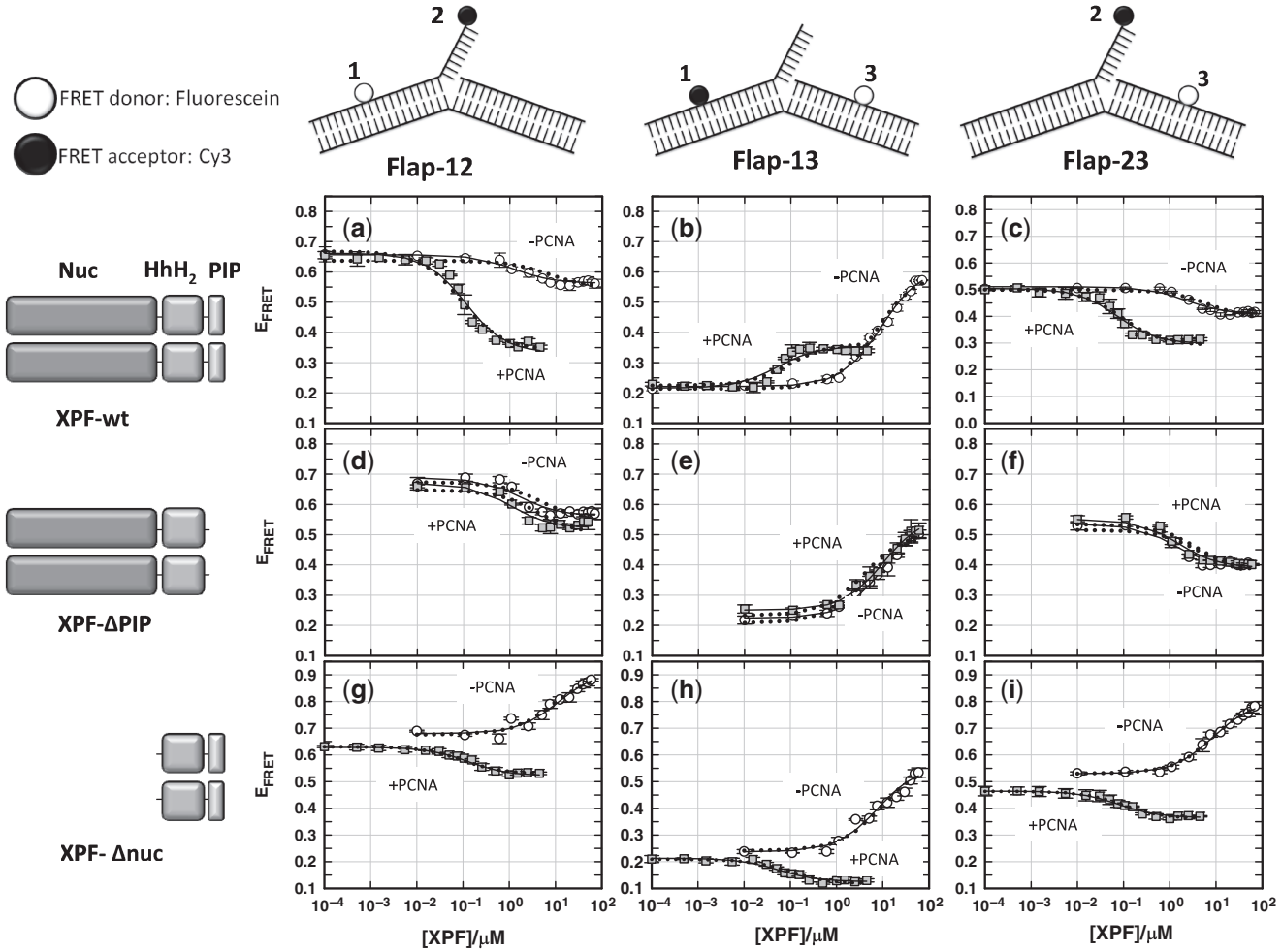

Figure 2. DNA distortion by XPF variants in the presence and absence of PCNA. Intermolecular FRET assay to monitor the interaction of XPF and truncated XPF variants (left column) with flap substrates labelled at the indicated positions (top row). Variation of FRET efficiencies for Flap-12 construct (column 1) at 20°C and 10 mM $CaCl_2$ as a function of (**a**) wild-type XPF (**d**) XPF-ΔPIP and (**g**) XPF-Δnuc concentration in the absence (white circles) and presence (grey squares) of 1 μM PCNA. Similar FRET assays under identical experimental conditions for Flap-13 and -23 are shown in columns 2 and 3 as a function of (**b, c**) wild-type XPF, (**e, f**) XPF-ΔPIP and (**h, i**) XPF-Δnuc in the absence (white circles) and presence (grey squares) of 1 μM PCNA. Individual fitting of the FRET-binding isotherm for each flap substrate using a one-site binding model described by Equation (1) ('Materials and Methods' section) are shown as continuous lines. Dotted lines represent the results obtained from a global fit of the three flap constructs for a given XPF protein. On the left, schematic representations of the three XPF variants used are shown.

Table 2. Summary of binding data obtained for the different FRET vectors studied in the presence of wild type XPF, and related mutants lacking the PCNA-interacting PIP box (XPF-ΔPIP) and the nuclease domain (XPF-Δnuc)

	Flap-12		Flap-13		Flap-23		Global Fit[a]	
	−PCNA	+PCNA[b]	−PCNA	+PCNA[b]	−PCNA	+PCNA[b]	−PCNA	+PCNA[b]
XPF-wt	2.6 ± 0.4	0.08 ± 0.01	9.2 ± 3	0.06 ± 0.01	5.0 ± 0.6	0.05 ± 0.01	5.3 ± 0.6	0.06 ± 0.01
XPF-ΔPIP	1.5 ± 0.5	1.6 ± 0.6	6.2 ± 0.7	3.2 ± 0.5	1.6 ± 0.2	1.8 ± 0.3	3.1 ± 0.5	2.7 ± 0.6
XPF-Δnuc	11 ± 3	0.17 ± 0.02	8 ± 2	0.09 ± 0.02	8.5 ± 1.2	0.10 ± 0.02	8 ± 1	0.11 ± 0.01

Dissociation constants are given in micromolar units.
[a]Results of a global fit including the three vectors for a given protein.
[b][PCNA] = 1.0×10^{-6} M.

vector with increasing concentrations of XPF or XPF variants in the presence and absence of PCNA. Dissociation constants for each FRET vector were obtained by fitting the FRET binding isotherm to Equation (1) ('Materials and Methods' section) which assumes a simple one-site binding model and 1:1 stoichiometry, and also estimated by globally fitting the three FRET vectors for a given protein. Data are shown graphically in Figure 2 and K_D values are listed in Table 2.

In the absence of PCNA, addition of wild type XPF induced significant changes in the FRET efficiency for all the vectors analysed, allowing the calculation of

Table 3. Values of donor–acceptor distances in angstroms obtained from FRET experiments for the different flap structures investigated in their complexes with XPF and XPF/PCNA

	Flap-12		Flap-13		Flap-23	
	−PCNA	+PCNA[a]	−PCNA	+PCNA[a]	−PCNA	+PCNA[a]
10 mM Ca^{2+}	50.2 ± 2.0	50 ± 1	69.6 ± 1.4	70 ± 1	55.6 ± 2.3	56 ± 1
XPF-wt	53.4 ± 0.8	61.8 ± 1.1	53.3 ± 1.3	62.1 ± 2.3	58.4 ± 1.3	63.8 ± 1.7
XPF-ΔPIP	53.7 ± 1.3	54.2 ± 1.8	55.1 ± 1.7	54.1 ± 2.4	59.6 ± 1.9	59.8 ± 1.4
XPF-Δnuc	41 ± 0.5	53.9 ± 2.9	54.7 ± 1.3	74.7 ± 2.8	45 ± 1	59.9 ± 1.6

[a][PCNA] = 1.0×10^{-6} M.

dissociation constants. These were of the same order of magnitude, with values of 2.6 ± 0.4, 9.2 ± 3.0 and 5.0 ± 0.6 μM for Flap-12, -13 and -23, respectively. Global modelling involving the three flaps yielded a K_D value of 5.3 ± 0.6 μM that fit accurately ($r^2 = 0.99$) all XPF-wt binding isotherms (Figure 2a–c). Although a systematic investigation of XPF binding affinities to different substrates is not available, the observed K_D is in the same range as reported for other HhH domain-containing proteins (7). For example, the C-terminal domain of UvrC binds with an apparent K_D of ∼1 μM to specific DNA substrates containing ss–ds junctions (29).

Experiments performed under identical conditions, but in the presence of 1 μM PCNA, show a strong effect on the XPF-wt binding affinity, yielding similar K_D values for the three FRET vectors (Table 2) and a global fitted value of 0.06 ± 0.01 μM, ∼90-fold lower than in the absence of PCNA. This value was very similar to that obtained when doing the reverse titration, 0.037 ± 0.007 μM, where PCNA binding was analysed in a background of XPF using the fluorescence quenching assay (Figure 1b) and to the K_M value of 0.08 ± 0.01 μM reported by us in a previous study (21). A similar affinity enhancement (∼73-fold) was observed for the XPF-Δnuc variant (Figure 2g–i) where global fit K_D values of 0.11 ± 0.01 and 8 ± 1 μM were obtained in the presence and absence of PCNA, respectively. These data highlight the major contribution of the C-terminal HhH_2 domain to DNA binding affinity. In marked contrast to XPF-wt and XPF-Δnuc, XPF-ΔPIP yielded global dissociation constants of 3.1 ± 0.5 μM in the presence and 2.7 ± 0.6 μM in the absence of PCNA (Figure 2d–f), confirming that the increase in affinity observed for wild-type XPF and XPF-Δnuc is due to the formation of a specific complex between these proteins and PCNA.

Structure of 3′-flap DNA substrates in their complexes with XPF and PCNA

XPF-induced FRET changes in the flap substrate. We next analysed in detail the variations in FRET efficiencies due to the interaction of XPF and related mutants with each of the flap substrate vectors. Control experiments performed for all the FRET vectors investigated showed that the fluorescence emission of an equivalent donor-only labelled substrate was partially quenched upon addition of XPF. The extent of quenching at saturating protein concentrations depended on the dye position. Thus, the experimental FRET efficiencies and associated inter-dye distances were corrected as described in 'Materials and Methods' section. For each experimental condition, three titrations were carried out to reduce the error in the observed FRET efficiency. The corresponding dye-to-dye distances are summarized in Table 3 and the mean E_{FRET} values shown as Supplementary Data (Supplementary Table S1). Relative changes in inter-dye distance upon association of XPF, with and without PCNA, are shown in Figure 3 for each vector analysed. In the absence of wild type XPF, the FRET efficiency obtained for Flap-12 substrate is 0.66 ± 0.02 and it decreased to a value of 0.58 ± 0.01 at saturating concentrations of XPF-wt (∼70 μM). This implies a moderate 3 Å increase in distance from 50.2 ± 2.0 to 53.4 ± 0.8 Å (Figure 3a). A similar decrease in FRET efficiency was also observed for the Flap-23 substrate upon addition of XPF-wt, from 0.51 ± 0.01 (55.6 ± 2.3 Å) in the absence of protein to a minimum value of 0.43 ± 0.02 (58.4 ± 1.3 Å) at saturating concentrations (Figure 3g). We obtained similar trends in FRET efficiencies for Flap-12 and -23 substrates containing 3-nt single-stranded flaps (data not shown), confirming that the observed variations were not due to environmental effects on the dyes upon XPF binding and were also independent of the flap length.

In contrast, Flap-13 undergoes an increase in E_{FRET} from 0.21 ± 0.03 to 0.57 ± 0.01 upon addition of wild-type XPF. When quantified, the average inter-dye distance for Flap-13 decreased by nearly 17, from 70 ± 1 Å with no added XPF to 53.3 ± 1.3 Å at saturating XPF concentrations (Figure 3d). Given that for Flap-13 both fluorophores are located in internal positions of the DNA substrate and to ensure that the FRET changes observed were not caused by a breakdown of the 2/3 approximation for the k^2 orientational factor when bound to XPF, we measured the donor anisotropy in the presence and absence of added XPF. We obtained values of 0.05 (no XPF-wt) and 0.18 (5 μM XPF-wt) indicating that the donor retains most of its mobility when bound to XPF and confirming that the FRET changes reflect XPF-induced variations in the Flap-13 average inter-dye distance. Assuming that XPF bends the flap substrate at the phosphate opposite the flap junction, and taking into account the position of the dyes, the dye-linker length, the helical structure of B-DNA, and the experimental inter-dye distances obtained by FRET, we obtained a model for the Flap-13 structure in the presence and absence of XPF. From this single-kink model, the kink angle changes

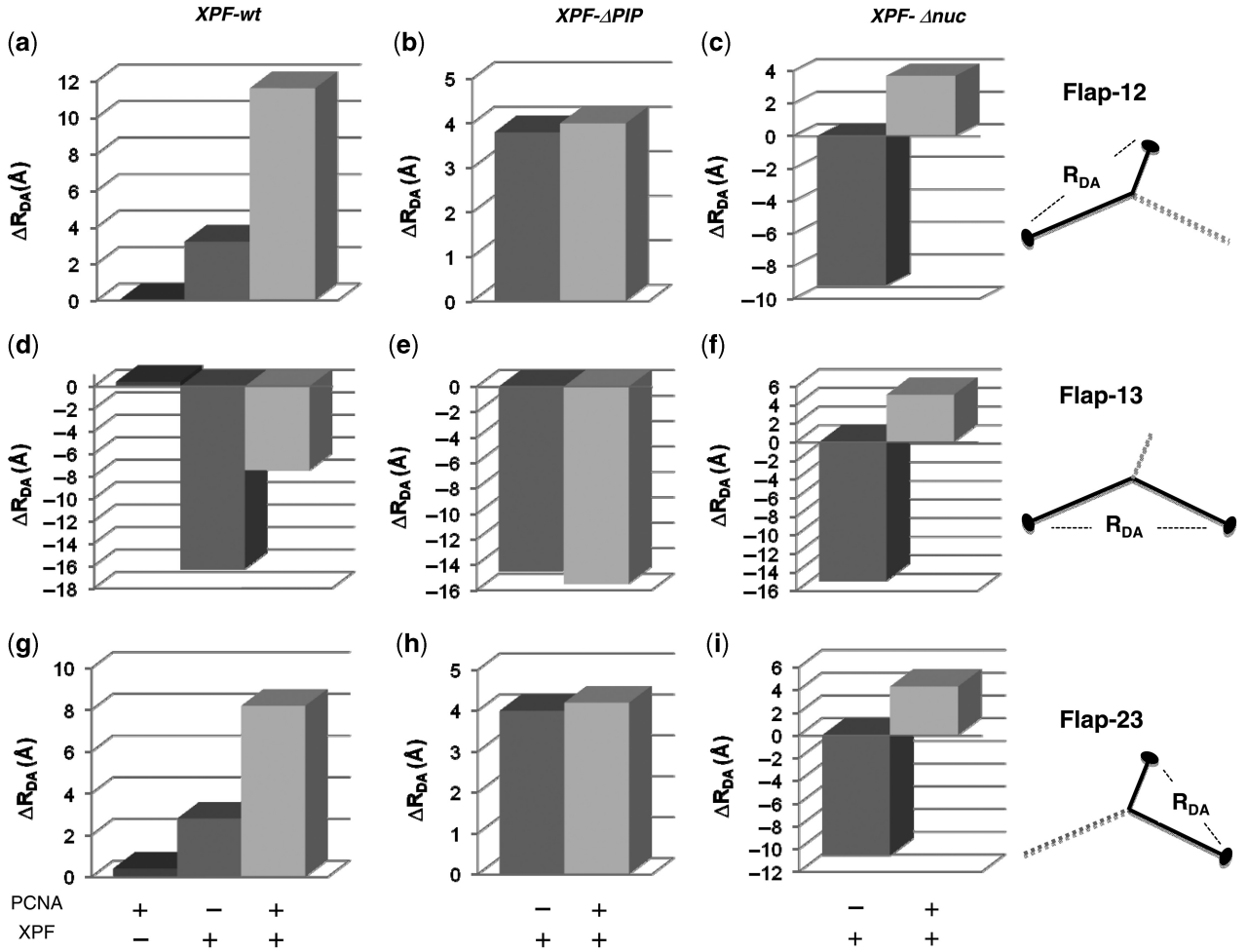

Figure 3. Comparison of relative changes in dye-to-dye distances (Å) observed for the three 3′ flap DNA constructs upon association to XPF and related variants in the presence and absence of PCNA. Dye-to-dye distances at 20°C in the presence of 10 mM $CaCl_2$ were evaluated from the FRET efficiencies obtained following the $(ratio)_A$ method (Materials and methods section). Relative distance changes where calculated with respect to the inter-dye distance obtained in the absence of proteins ($\Delta R = R_{protein} - R_{free}$), with positive and negative ΔR values representing an increase or a decrease in inter-dye distance, respectively. Top panels: relative change in dye-to-dye distance obtained for Flap-12 upon association to XPF-wt (**a**), XPF-ΔPIP (**b**) and XPF-Δnuc (**c**). Middle panels: relative change in dye-to-dye distance obtained for Flap-13 upon association to XPF-wt (**d**), XPF-ΔPIP (**e**) and XPF-Δnuc (**f**). Bottom panels: relative change in dye-to-dye distance distances obtained for Flap-23 upon association to XPF-wt (**g**), XPF-ΔPIP (**h**) and XPF-Δnuc (**i**).

from 157° to ~93° upon association of XPF. This value is in very good agreement with the kink angle of ~90° estimated for the XPF/DNA complex using a combination of modeling and X-ray data (8) and with the kink angle observed for a 5′flap DNA substrate bound to Fen-1 using a similar FRET approach (10).

For XPF-ΔPIP, the relative change in dye-to-dye distance obtained for the three flap constructs were very similar to those observed for XPF-wt (Figure 3b, e and h). Hence, XPF-ΔPIP distorts the DNA flap in the same manner as the wild type. However, similar experiments carried out with XPF-Δnuc showed that whilst Flap-13 FRET distance (Figure 3f) was similar to that reported for XPF-wt (Figure 3d), Flap-12 (Figure 3c) and Flap-23 (Figure 3i) exhibited an opposite effect. Upon XPF-Δnuc binding, Flap-12 E_{FRET} increased from 0.66 ± 0.02 to 0.87 ± 0.03 and Flap-23 from 0.51 ± 0.01 to 0.79 ± 0.03. These FRET efficiencies at saturating XPF-Δnuc concentrations correspond to dye-to-dye distances of 41 ± 0.5 Å (Flap-12) and 45 ± 1 Å (Flap-23), much shorter than those induced by XPF-wt. Together these data suggest that the C-terminal HhH_2 domains are responsible for duplex DNA bending whilst the nuclease domains must contribute to organise the flap substrate in a proper conformation for recognition and cleavage.

Flap conformation in presence of the XPF/PCNA complex. FRET changes occurring upon titration of XPF were also performed in the presence of 1 μM PCNA. Although the FRET efficiency curves as a function of XPF-wt concentration followed a similar pattern as in the absence of PCNA (Figure 2a–c), the plateau values obtained at saturating XPF-wt concentrations (~5 μM) were significantly lower (Table 1, Supplementary Data). Thus, the E_{FRET} for Flap-12

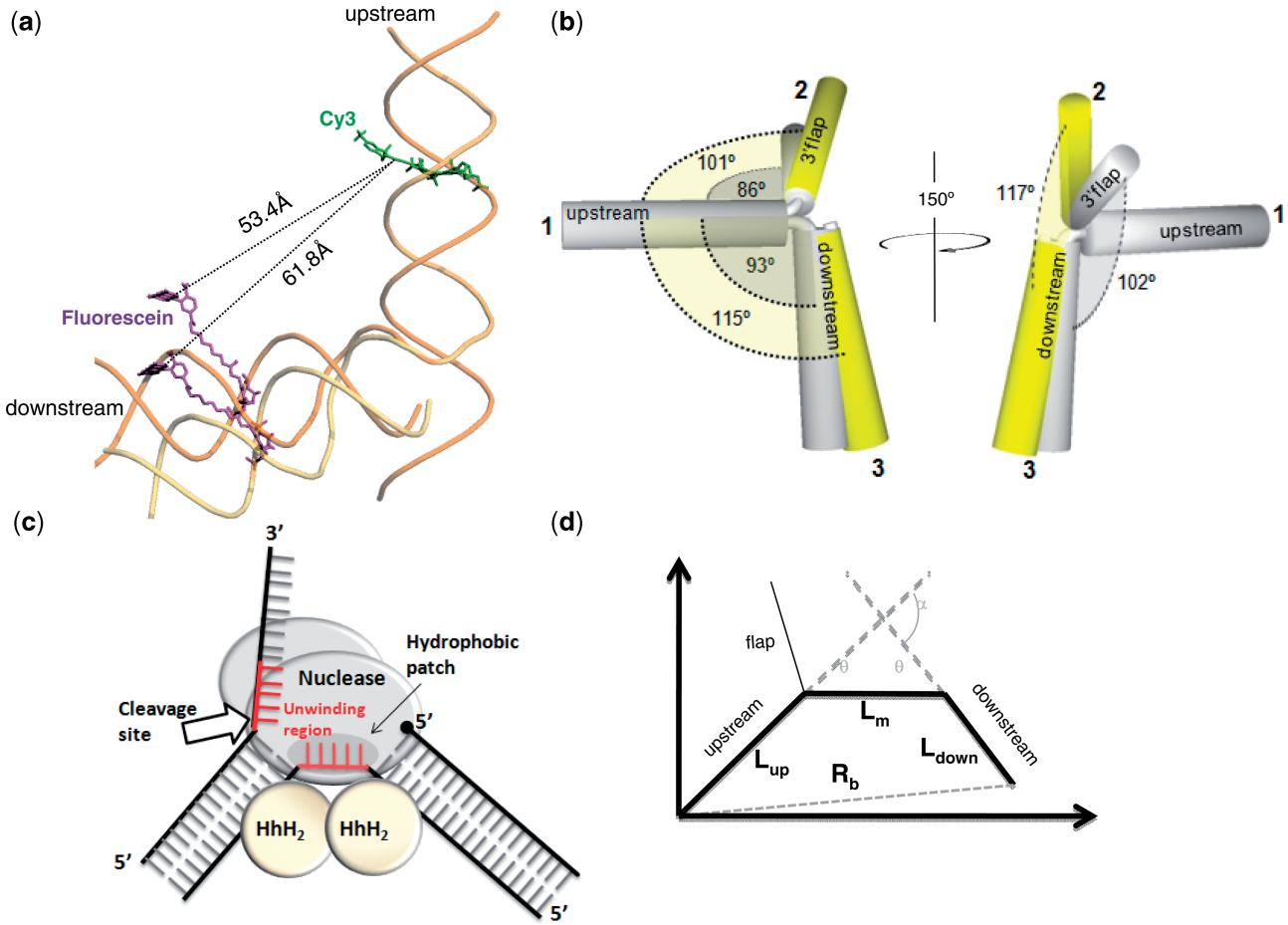

Figure 4. Architecture of the DNA substrate in its complexes with XPF and XPF/PCNA. (**a**) Model of the flap substrate showing the relative position of the fluorescein donor (magenta) and the Cy3 acceptor (green) obtained from the FRET assay when bound to XPF (dark orange) and XPF/PCNA (light orange). The up- and down-stream duplexes were built using canonical B-DNA parameters with the base-pair sequence matching the substrate sequence used in this work. The 8-nt 3′ substrate overhang was built as a single-strand of canonical B-DNA with an A nucleotide followed by a T-repeat sequence of 7-nt. The dye-linker structure of fluorescein and Cy3 has been built and energy minimized using HyperChem v.8 and then joined to the DNA structure at the appropriate location. The downstream duplex region was positioned using the distance dye-to-dye distance information extracted from the FRET experiments whilst keeping the upstream duplex at a fixed position. (**b**) Cartoon representing the conformational distortions taking place on the flap structure bound to XPF (grey) upon association to PCNA (yellow) assuming a single-kink model (see text for details) and an inter-nucleotide distance of 5.3 Å as obtained from the average of six crystal structures of single-strand/protein complexes (see text). (**c**) Structural basis for a double-kink model (8,15). Cartoon shows the two HhH_2 domains engaging the upstream and downstream duplexes to induce a 90° global kink angle, whilst the uncleaved strand linking both duplexes interacts with the nuclease domain promoting melting of the upstream duplex. (**d**) Parameters involved in the double-kink model used to calculate the angle α to which XPF kinks the DNA substrate. The DNA has been modelled as a rod consisting of three segments, L_{up}, L_{down} and L_m, accounting for the up-, downstream and ss regions, respectively. The model is similar to that reported for the analysis of DNA bending by TBP (23).

decreased from 0.58 ± 0.01 with no PCNA added to a value of 0.36 ± 0.01 with PCNA, and from 0.57 ± 0.01 and 0.43 ± 0.02 to values of 0.35 ± 0.01 and 0.31 ± 0.02 for Flap-13 and Flap-23, respectively. The dye-to-dye distances for the three flap substrates bound to the XPF/PCNA complex were extracted from the FRET efficiencies and compared to those observed when bound to XPF alone (Table 3). Flap-12 and -13 showed similar 16% increase in inter-dye distance, from 53.4 ± 0.8 and 53.3 ± 1.3 with no added PCNA to 61.8 ± 1.1 and 62.1 ± 2.3 in the presence of XPF/PCNA, respectively. For Flap-23 the inter-dye distance increased by 10% from 58.4 ± 1.3 when bound to XPF to a value of 63.8 ± 1.7 in the presence of the XPF/PCNA complex (Figure 4a). Using the single-kink model and the inter-dye distance obtained from the FRET assay in the presence of XPF/PCNA complex, we obtained a kink angle of 115° between the up- and downstream duplexes. This represents an increase in the kink angle by nearly 23° with XPF/PCNA when compared to XPF alone. As a control, when the concentration of XPF-ΔPIP variant was increased from 0 to 70 μM in the presence of 1 μM PCNA, the E_{FRET} followed the same variation and reached the same plateau values as in the absence of PCNA. We conclude that the observed conformational changes are triggered by the specific interaction of the DNA substrate with the XPF/PCNA complex. The flap structure bound to the XPF-Δnuc variant was also investigated in the presence of PCNA (Figure 2g–i). The three flap substrates exhibited a decrease in FRET

efficiency as XPF-Δnuc was titrated in the presence of 1 μM PCNA. At saturating XPF-Δnuc concentrations the E_{FRET} values obtained were 0.55 ± 0.02 (Flap-12), 0.15 ± 0.03 (Flap-13) and 0.38 ± 0.02 (Flap-23). The inter-dye distances extracted from these values are listed in Table 3. It is clear that XPF-Δnuc/PCNA distorts the flap substrate in a very different manner than the complex XPF-wt/PCNA, and this appears to be attributable to the lack of the nuclease domain.

These findings provide the first, to our knowledge, experimental evidence that PCNA association can lead to a substantial reorganization of a DNA substrate, suggesting that the sliding clamp can have an active role in the modulation of DNA structure in collaboration with partner proteins. This is consistent with a model where PCNA acts not only as a protein-recruiter of XPF to the flap ss/ds junction but also as molecular scaffold that enables XPF to further reorganize the DNA substrate, towards a more catalytically competent structure, first proposed on the basis of kinetic studies of this system (21). Similar dual functionalities have recently been indentified for TFIIA cofactors in the context of eukaryotic mRNA transcription (23).

DISCUSSION

XPF and PCNA assemble in a defined orientation on flap DNA substrates

Despite much interest, structural information regarding the interaction of the PCNA with the nucleic acid scaffold and the overall orientation of the sliding clamp relative to the DNA damage site in the presence and absence of a given protein partner is very limited. Here, we developed a fluorescence assay that used PCNA-induced quenching of fluorescein emission to analyse the organization of the PCNA–DNA complex in the presence and absence of XPF. The extreme sensitivity of fluorescein to its microenvironment has been used previously for the analyses of protein–DNA interactions (30). Our data suggest a model where PCNA on its own can assemble randomly with a 1:1 stoichiometry and equal affinity at either side of the 3′ flap substrate, as reflected by the identical quenching (~30%) exhibited by a fluorescein dye located at almost symmetrical positions, either on the upstream (11-nt) or on the downstream duplex (10-nt), and by the similar dissociation constants obtained (Figure 1b). It has been proposed that *Escherichia coli* β sliding clamp and human PCNA can transverse small DNA secondary structures including short flap structures of 10-nt, being efficiently blocked by longer flaps (~28-nt) (31). Thus, we cannot rule out the possibility that the observed spontaneous assembly of PCNA at either side of the flap substrate could be coupled to PCNA sliding over the eight nucleotide ss flap used in this study. Although currently there are no data available to further confirm this aspect, the proposed architectural model remains unaffected. Similar random orientation has been observed previously for the assembly of mammalian PCNA on a DNA template-primer containing a ds/ss junction (32).

In the presence of XPF, *a priori*, one could envisage two possible arrangements for PCNA on the DNA flap substrate: PCNA could be loaded onto the duplex upstream of XPF or downstream. The strong bias in fluorescein quenching by PCNA in the presence of XPF provides clear evidence for an XPF-directed assembly of PCNA exclusively onto the upstream region (Figure 1b). Preferential PCNA loading onto the upstream region also provides a mechanistic explanation for the observed activation of XPF activity by PCNA in gapped and splayed substrates, as the upstream region is the only DNA duplex close to the enzyme complex in these structures (15).

PCNA and XPF cooperate to bind DNA substrates

To dissect the role that the sliding clamp plays in XPF recognition and cleavage, we have used FRET assays to quantify the affinity of XPF for its preferred substrates, 3′ DNA flaps, with and without PCNA. The dissociation constants obtained using a global fit analysis of the three flap vectors (K_D = 5.3 ± 0.6 μM) was very similar to those obtained for the binding of PCNA to the upstream (8.5 ± 1.6 μM) and downstream duplexes (6.9 ± 1.8 μM), and for the interaction between XPF and PCNA determined previously using isothermal titration calorimetry (3.8 ± 0.6 μM) (21). The 90-fold decrease in the dissociation constant for DNA binding by XPF in the presence of 1 μM PCNA reflects the energetically favorable interactions XPF can make with both PCNA and DNA. The C-terminal HhH_2 domain of XPF yielded values similar to those for full length enzyme, suggesting that the nuclease domain contributes little to DNA binding. In vivo, PCNA is likely to be pre-loaded onto duplex DNA by the RFC complex and will arrive at non-canonical DNA structure by 1D diffusion or during the course of DNA replication. On encountering a branched DNA structure PCNA may stall or at least pause, allowing recruitment of an endonuclease competent to process the DNA. In the absence of PCNA, XPF will bind very weakly to branched substrates; PCNA is therefore essential in 'marking' potential substrates for nuclease action, but in the case of XPF it has a further role which is discussed below.

Structural organization of XPF/DNA complexes

For both HhH_2 domains to engage in interactions with the upstream and downstream duplex simultaneously, it has been proposed that the 3′ flap substrate would have to bend by almost 90° (6,8). However, the crystal structure of ApeXPF bound to the DNA substrate contained only the downstream DNA motif and thus no quantitative experimental evidence of this or other XPF-induced conformational changes on the flap substrate have been reported to date. To investigate the conformational changes taking place on the DNA substrate upon binding of XPF, we translated the observed FRET efficiencies in inter-dye distances. Of all the flap structures investigated, the duplex-bending reporter Flap-13 showed the highest relative change in dye-to-dye distance (~16 Å) upon XPF binding. This was in contrast with the very moderate relative increase in distance (~3 Å) obtained

for Flap-12 and -23 (Table 3), which report conformational changes between the duplex and flap regions. The decrease in the distance associated with Flap-13 can be explained by a kink centered at the phosphate opposite the flap junction acting as a flexible hinge, resulting in an angle of 93° between the upstream and downstream regions (Figure 4a). This value is similar to that proposed for Fen-1, whose activity is also known to be PCNA-activated (10). Thus, a kinked DNA conformation seems to arise as a common feature in the recognition mechanism of branched DNA structures. Sharply kinked protein-induced DNA structures have been also proposed for the UvrB helicase (33) and for nick recognition by the NAD^+-dependent DNA ligase from *T. filiformis* (34).

Although the single-kink model provides an appropriate explanation for the conformational changes observed on the DNA upon XPF binding and agrees with the deformation model proposed for other endonucleases such as Fen-1, it does not contemplate additional interactions between the XPF nuclease domain and the flap substrate observed on the ApeXPF cocrystal structure and also suggested by biochemical methods (8,15). According to this, a hydrophobic strip on the surface of the nuclease domain is predicted to function as a binding site for the ssDNA linking the upstream and downstream duplexes, generating a small stretch of unpaired ssDNA in the substrate strand that is cleaved in the nuclease active site (Figure 4c). This XPF-induced melting of the DNA substrate is consistent with footprinting data that demonstrate opening of a DNA duplex near the cleavage site by the Hef protein (6), a 'long form' analog of XPF present in most euryarchaea. Thus, the overall organization of the HhH_2 and nuclease domains around the DNA substrate could be reminiscent of double-kink models proposed for DNA bending enzymes such as the TATA binding protein (TBP) (23) and the CENP-B/DNA complex (35), among others.

To envision whether DNA-melting associated to the interaction between the nuclease domain and the flap substrate could account for the changes in dye-to-dye distances observed for Flap-13, we applied a similar model to the XPF/DNA complex (Figure 4d). The proposed double-kink structure is characterized by an overall kink angle α assumed to be 90° as explained above, two equal kinks of exterior angle occurring at the ss/dsDNA hinges so that $\alpha = 2$, the distance R_b that corresponds to the inter-dye distance when bound to XPF, experimentally obtained by FRET, and the lengths L_{down}, L_{up} and L_m whose magnitudes correspond to the downstream, upstream and the unpaired segments, respectively. An intrinsic uncertainty in this model arises from the inter-base distance to be assigned for the single-strand region (L_m) with literature values ranging from 4 Å (36) to 5.6 Å (37). Thus, to estimate L_m, we first calculate an average inter-nucleotide distance using crystal structures of ssDNA bound to different proteins including DNA polymerase β (PDB code 9ICM), NS3 helicase (PDB code 1A1V), *E. coli* Rep helicase (PDB code 1UAA), *E. coli* SSDNA (PDB code 1EYG) and human RPA (PDB code 1JMC). We obtained an average value of 5.3 ± 0.7 Å, which is close to the average rise of 5.1 Å per nucleotide reported for ssDNA bound to RecA (38). Using this value and the double-kink model, the experimental FRET distance of 53.3 ± 1.3 Å would be compatible with a ssDNA linker L_m extending ~4-nt between the upstream and the downstream duplexes. Interestingly, biochemical data have previously shown that the XPF (15) and Mus81-Mms4 (39) cleavage site is located 4–5-nt from the 5′-end of the downstream duplex. Hence, we suggest that melting of the upstream duplex to position the flap substrate in an optimal conformation ready for cleavage might reflect a fundamental conserved element in the DNA processing pathway for both enzymes.

Surprisingly, the DNA substrate bound to the XPF variant lacking the nuclease domain (XPF-Δnuc) shows a very different organization (Figure 3c, f and i) with Flap-12 and -23 inter-dye distances being much shorter than those obtained when bound to the full length XPF. This suggests that the nuclease domain plays an important role to position the flap substrate in the proper conformation.

PCNA alters the conformation of XPF/DNA complexes

In the presence of PCNA, the inter-dye distances obtained for the three flap constructs were higher than in the presence of XPF-wt alone (Table 3). Flap-12 and -13 both showed increases of ~17 %, whilst Flap-23 showed only a 9% increase (Figure 3a, d and g). The observed changes in DNA conformation are due to the formation of a specific complex between XPF and PCNA, as the truncated XPF-ΔPIP, unable to interact with PCNA, showed similar dye-to-dye distances to that reported only with XPF-wt (Figure 3b, e and h). This is in agreement with our observation that the last six C-terminal residues of XPF mediate the interface with PCNA and with the lack of PCNA stimulation of nuclease activity previously reported for XPF-ΔPIP (16). Using the single-kink model, we found that the angle for Flap-13 increases from 93° in the absence of XPF to 115° upon the association of PCNA. Flap-12 and -23 also undergo a PCNA-induced opening of the corresponding angle, from 86° to 101° and from 102° to 117°, respectively (Table 2, Supplementary Data). Hence, we suggest that PCNA association promotes an additional reorganization of the DNA flap substrate beyond that induced by XPF-wt alone. A single-kink model of the flap substrate based on the inter-dye distances and angles obtained for the XPF/DNA complex in the presence and absence of PCNA is shown in Figure 4b, assuming a ss internucleotide distance of 5.3 Å. Alternatively, applying the double-kink model (Figure 4c and d) and the average inter-nucleotide distance of 5.3 Å, we found that the FRET distance obtained for the Flap-13 substrate bound to XPF and PCNA is compatible with a ss melted region covering ~6–7 nucleotides between the up- and the downstream duplexes, which represents 2–3 nt additional melting compared to XPF-wt alone. For comparison, values of 9 and ~5–6 nt were obtained using the limiting values of 4 and 5.6 Å reported in the literature for the inter-base distance. In these calculations

we have kept the kink-angle constant at 90° and assumed that the distance changes are exclusively caused by an increased upstream melting in the presence of PCNA. Our data do not allow us to further evaluate whether the relative changes in distance arise exclusively from unwinding, from a modification of the kink angle induced by PCNA binding, or from a combination of both. However, they demonstrate that PCNA association leads to a different relative positioning of the up- and down-stream complexes when compared to that in the complex XPF/DNA. These data are consistent with the kinetic studies which demonstrated an essential role for PCNA in the catalytic cycle of crenarchaeal XPF (21).

In summary, we have demonstrated that XPF recognition of the DNA flap substrate requires both the nuclease and HhH_2 domains to act in a concerted manner to position the DNA structure in the proper conformation for cleavage. Our data confirm that XPF distorts the substrate mostly by inducing a 90° kink angle between the down- and upstream regions as predicted from the ApeXPF cocrystal (8). Moreover, for the first time, we provide experimental evidence showing that the structure of the XPF/DNA complex is markedly different in the presence and absence of PCNA. Our model underlines the significant role that PCNA plays as a molecular scaffold, enabling XPF to further distort the DNA structure, and points towards the XPF/PCNA unit as the active complex. The absolute requirement of PCNA for XPF activity, together with this novel dimension of PCNA function coordinating the XPF-induced deformation of the flap substrate, might represent a finely tuned quality control mechanism, designed to ensure that cleavage only occurs when the DNA damage is recognized correctly by the repair machinery. Given the ubiquity of PCNA in DNA processing pathways and the ever growing number of endonucleases and other proteins whose function is known to be stimulated by PCNA, our findings provide a framework to understand PCNA function beyond a hand-off platform where proteins are transiently exchanged.

SUPPLEMENTARY DATA

Supplementary Data are available at NAR Online.

ACKNOWLEDGEMENTS

The authors thank Catherine Botting and the St Andrews University Mass Spectrometry facility for analyses, and Paul Talbot and Biljana Petrovic-Stojanovska for technical support.

FUNDING

Biotechnology and Biological Sciences Research Council Grant number BB/D001439/1 and BB/E014671/1. Funding for open access charge: University of St Andrews.

Conflict of interest statement. None declared.

REFERENCES

1. Nishino,A.J. and Morikawa,K. (2002) Structure and function of nucleases in DNA repair: shape, grip and blade of the DNA scissors. *Oncogene*, **21**, 9022–9032.
2. Nishino,T., Ishino,Y. and Morikawa,K. (2006) Structure-specific DNA nucleases: structural basis for 3D scissors. *Curr. Op. Struct. Biol.*, **16**, 60–67.
3. de Laat,W.L., Appeldoorn,E., Jaspers,N.G.J. and Hoeijmakers,J.H.J. (1998) DNA structural elements required for ERCC1-XPF endonuclease activity. *J. Biol. Chem.*, **273**, 7835–7842.
4. Lehmann,A.R. (2003) DNA repair-deficient diseases, xeroderma pigmentosum, Cockayne syndrome and trichothiodystrophy. *Biochimie*, **85**, 1101–1111.
5. Roberts,J. and White,M.F. (2004) An Archaeal endonuclease displays key properties of both eukaryal XPF-ERCC1 and Mus81. *J. Biol. Chem.*, **280**, 5924–5928.
6. Nishino,T., Komori,K., Ishino,Y. and Morikawa,K. (2005) Structural and functional analyses of an Archaeal XPF/Rad1/Mus81 nuclease: asymmetric DNA binding and cleavage mechanisms. *Structure*, **13**, 1183–1192.
7. Tsodikov,O.V., Enzlin,J.H., Schärer,O.D. and Ellenberger,T. (2005) Crystal structure abd DNA binding functions of ERCC1, a subunit of the DNA structure-specific endonuclease XPF-ERCC1. *Proc. Natl Acad. Sci. USA*, **102**, 11236–11241.
8. Newman,M., Murray-Rust,J., Lally,J., Rudolf,J., Fadden,A., Knowles,P.P., White,M.F. and McDonald,N.Q. (2005) Structure of an XPF endonuclease with and without DNA suggests a model for substrate recognition. *EMBO J.*, **24**, 895–905.
9. Ariyoshi,M., Nishino,T., Iwasaki,H. and Morikawa,K. (2000) Crystal structure of the holliday junction DNA in complex with a single RuvA tetramer. *Proc. Natl Acad. Sci. USA*, **97**, 8257–8262.
10. Chapados,B.R., Hosfield,D.J., Han,S., Qiu,J., Yelent,B., Shen,B. and Tainer,J.A. (2004) Structural basis for Fen-1 substrate specificity and PCNA-mediated activation in DNA replication and repair. *Cell*, **116**, 39–50.
11. Frank,G., Qiu,J., Zheng,L. and Shen,B. (2001) Stimulation of eukaryotic flap endonuclease-1 activities by proliferating cell nuclear antigen (PCNA) is independent of its in vitro interaction via a consensus PCNA binding region. *J. Biol. Chem.*, **276**, 36295–36302.
12. Tom,S., Henricksen,L.A. and Bambara,R.A. (2000) Mechanism whereby proliferating cell nuclear antigen stimulates flap endonuclease 1. *J. Biol. Chem.*, **275**, 10498–10505.
13. Vivona,J.B. and Kelman,Z. (2003) The diverse spectrum of sliding clamp interacting proteins. *FEBS Lett.*, **546**, 167–172.
14. Moldovan,G.L., Pfander,B. and Jentsch,S. (2007) PCNA, the maestro of the replication fork. *Cell*, **129**, 665–679.
15. Roberts,J.A. and White,M.F. (2005) DNA end-directed and processive nuclease activities of the archaeal XPF enzyme. *Nucleic Acids Res.*, **33**, 6662–6670.
16. Roberts,J.A., Bell,S.D. and White,M.F. (2003) An archaeal XPF repair endonuclease dependent on a heterotrimeric PCNA. *Mol. Microbiol.*, **48**, 361–371.
17. Dionne,I., Nookala,R.K., Jackson,S.P., Doherty,A.J. and Bell,S.D. (2003) A heterotrimeric PCNA in the hyperthermophylic archaeon *Sulfolobus Solfataricus*. *Mol. Cell*, **11**, 275–282.
18. Williams,G.J., Johnson,K., Rudolf,J., McMahon,S.A., Carter,L., Oke,M., Liu,H., Taylor,G.L., White,M.F. and Naismith,J.H. (2006) Structure of the heterotrimeric PCNA from *Sulfolobus Solfataricus*. *Acta crystallogr.*, **62**, 944–948.
19. Dore,A.S., Kilkenny,M.L., Jones,S.A., Oliver,A.W., Roe,S.M., Bell,S.D. and Pearl,L.H. (2006) Structure of an archaeal PCNA1-PCNA2-FEN1 complex: elucidating PCNA subunit and client specificity. *Nucleic Acids Res.*, **34**, 4515–4526.
20. Pascal,J.M., Tsodikov,O.V., Hura,G.L., Song,W., Cotner,E.A., Classen,S., Tomkinson,A.E., Tainer,J.A. and Ellenberger,T. (2006) A flexible interface between DNA ligase and PCNA supports conformational switching and efficient ligation of DNA. *Mol. Cell*, **24**, 279–291.
21. Hutton,R.D., Roberts,J.A., Penedo,J.C. and White,M.F. (2008) PCNA stimulates catalysis by structure-specific nucleases using

two distinct mechanisms: substrate targeting and catalytic step. *Nucleic Acids Res.*, **36**, 6720–6727.
22. Clegg,R.M. (1992) Fluorescence resonance energy transfer and nucleic acids. *Methods Enzymol.*, **211**, 353–388.
23. Hieb,A.R., Halsey,W.A., Betterton,M.D., Perkins,T.T., Kugel,J.F. and Goodrich,J.A. (2007) TFIIA changes the conformation of the DNA in TBP/TATA complexes and increases their kinetic stability. *J. Mol. Biol.*, **372**, 619–632.
24. Steinmetzer,K., Behlke,J., Brantl,S. and Lorenz,M. (2002) CopR binds and bends its target DNA: a footprinting and fluorescence resonance energy transfer study. *Nucleic Acids Res.*, **30(9)**, 2052–2060.
25. Gryczynski,I., Wiczk,W., Johnson,M.L., Cheung,H.C., Wang,C.-K. and Lakowicz,J.F. (1988) Resolution of end-to-end distance distributions of flexible molecules using quenching-induced variations of the Förster distance for fluorescence resonance energy transfer. *Biophys. J.*, **54**, 577–586.
26. Tang,G.-Q. and Patel,S. (2006) T7 RNA polymerase-induced bending of promoter DNA is coupled to DNA opening. *Biochemistry*, **45**, 4936–4946.
27. Rao,H.G.V., Rosenfeld,A. and Wetmur,J.G. (1998) Methanococuss jannaschii flap endonuclease: expression, purification and substrate requirements. *J. Bacteriol.*, **148**, 5406–5412.
28. Okahata,Y., Kitamura,Y., Hagimara,N. and Furusawa,H. (2000) Quantitative detection of binding of PCNA proteins to DNA strands on a 27 MHz quartz crystal microbalance. *Nucleic Acids Symp. Ser.*, **44**, 243–244.
29. Singh,S., Folkers,G.E., Bonvin,A.M.J.J., Boelens,R., Wechselberger,R., Niztayev,A. and Kaptein,R. (2002) Solution structure and DNA-binding properties of the C-terminal domain of UvrC from E coli. *EMBO J.*, **21**, 6257–6266.
30. Drees,B.L., Rye,H.S., Glazer,A.N. and Nelson,H.C.M. (1996) Environment-sensitive labels in multiplex fluorescence analyses of protein-DNA complexes. *J. Biol. Chem.*, **271**, 32160–32173.
31. Yao,N., Hurwitz,J. and O'Donnell,M. (2000) Dynamics of β and proliferating cell nuclear antigen in traversing DNA secondary structure. *J. Biol. Chem.*, **275**, 1421–1432.
32. Mozzherin,D.J., Tan,C.-K., Downey,K.M. and Fisher,P.A. (1999) Architecture of the active DNA polymerase δ•Proliferating cell nuclear antigen•Template-primer complex. *J. Biol. Chem.*, **274**, 19862–19867.
33. Shi,Q., Thresher,R., Sancar,A. and Griffith,J. (1992) Electron microscopy study of (A)BC excinuclease. DNA is sharply bent in the UvrB-DNA complex. *J. Mol. Biol.*, **226**, 425–432.
34. Lee,Y.J., Chang,C., Song,H.K., Moon,J., Yang,J.K., Kim,H.-K., Kwon,S.-T. and Suh,S.W. (2000) Crystal structure of NAD + -dependent DNA ligase: modular architecture and functional implications. *EMBO J.*, **19**, 1119–1129.
35. Tanaka,Y., Nureki,O., Kurumizaka,H., Fukai,S., Kawaguchi,S., Ikuta,M., Iwahara,J., Okazaki,T. and Yokoyama,S. (2001) Crystal structure of the CENP-B protein-DNA complex: the DNA-binding domains of CENP-B induce kinks in the CENP-B box DNA. *EMBO J.*, **20**, 6612–6618.
36. Soengas,M.S., Reyes-Mateos,C., Rivas,G., Salas,M., Acuna,A.U. and Gutierrez,C. (1997) Structural features of ϕ29 single-stranded DNA-binding protein. *J. Biol. Chem.*, **272**, 303–310.
37. Smith,S.B., Cui,Y. and Bustamante,C. (1996) Overstretching B-DNA: The elastic response of individual double-stranded and single-stranded DNA molecules. *Science*, **271**, 795–799.
38. Yu,X., Jacobs,S.A., West,S.C., Ogawa,T. and Egelman,E.H. (2001) Domain structure and dynamics in the helical filaments formed by RecA and Rad51 on DNA. *Proc. Natl Acad. Sci. USA*, **98**, 8419–8424.
39. Bastin-shanower,S.A., Fricke,W.M., Mullen,J.R. and Brill,S.J. (2003) The mechanism of Mus81-Mms4 cleavage site selection distinguishes it from the homologous endonuclease Rad1-Rad10. *Mol. Cell. Biol.*, **23**, 3487–3496.